PASJ: Publ. Astron. Soc. Japan **60**, 577–585, 2008 June 25
© 2008. Astronomical Society of Japan.

Cooperative Observation of Ellerman Bombs between the Solar Optical Telescope aboard Hinode and Hida/Domeless Solar Telescope

Takuma MATSUMOTO,[1,2] Reizaburo KITAI,[2] Kazunari SHIBATA,[2] Shin'ichi NAGATA,[2] Kenichi OTSUJI,[1,2]
Tahei NAKAMURA,[1,2] Hiroko WATANABE,[1,2] Saku TSUNETA,[3] Yoshinori SUEMATSU,[3] Kiyoshi ICHIMOTO,[3]
Toshifumi SHIMIZU,[4] Yukio KATSUKAWA,[3] Theodore D. TARBELL,[5] Bruce W. LITES,[6]
Richard A. SHINE,[5] and Alan M. TITLE[5]

[1]*Department of Astronomy, Kyoto University, Kitashirakawa-Oiwake-cho, Sakyo-ku, Kyoto 606-8502*
[2]*Kwasan and Hida Observatories, Kyoto University, Yamashina-ku, Kyoto 607-8471*
mtakuma@kwasan.kyoto-u.ac.jp
[3]*National Astronomical Observatory of Japan, 2-21-1 Osawa, Mitaka, Tokyo 181-8588*
[4]*Institute of Space and Astronautical Science, Japan Aerospace Exploration Agency, 3-1-1 yoshinodai, Sagamihara, Kanagawa 229-8510*
[5]*Lockheed Martin Advanced Technology Center, Palo Alto, CA 94304, USA*
[6]*High Altitude Observatory, 3450 Mitchell Lane, Boulder, CO 80301, USA*

(Received 2007 May 31; accepted 2008 January 31)

Abstract

High-resolution Ca II H broad-band filter images of NOAA 10933 on 2007 January 5 were obtained by the Solar Optical Telescope aboard the Hinode satellite. Many small-scale ($\sim 1''$) bright points were observed outside the sunspot and inside the emerging flux region. We identified some of these bright points with Ellerman bombs (EBs) by using Hα images taken by the Domeless Solar Telescope at Hida observatory. The sub-arcsec structures of two EBs seen in Ca II H were studied in detail. Our observation showed the following two aspects: (1) The Ca II H bright points identified with EBs were associated with the bipolar magnetic field structures, as reported by previous studies. (2) The structure of the Ca II H bright points turned out to consist of the following two parts: a central elongated bright core ($0.''7 \times 0.''5$) located along the magnetic neutral line and a diffuse halo ($1.''2 \times 1.''8$).

Key words: Sun: activity — Sun: atmospheric motions — Sun: chromosphere — Sun: magnetic fields — Sun: photosphere

1. Introduction

Ellerman bombs (EBs: Ellerman 1917) are known as chromospheric phenomena that have characteristic Hα spectra: broad emission lines with central absorption lines. The typical size of EBs is on the order of $1''$, and generally EBs last for 10–14 min. EBs generally occur in newly developed emerging flux regions, or at the edge of penumbrae. Although many studies have revealed the basic properties of EBs (Roy 1973; Kurokawa et al. 1982; Kitai 1983; Kitai & Muller 1984; Zachariadis et al. 1987; Nindos & Zirin 1998; Georgoulis et al. 2002; Pariat et al. 2004), their triggering mechanism has not yet been clearly understood.

Kitai (1983) showed that non-LTE calculations of a perturbed, heated, and condensed chromosphere reproduced well-observed Hα profiles. Ding, Hénoux, and Fang (1998) and Hénoux, Fang, and Ding (1998) also reproduced profiles of EBs by considering energetic particle beams bombarding the atmosphere. Both studies have suggested that heating lower atmospheres, such as the lower chromosphere, plays an important role in producing Hα profiles of EBs.

Pariat et al. (2004) suggested that magnetic reconnection at magnetic dips in undulatory magnetic field of emerging flux region is the triggering mechanism of EBs. Matsumoto et al. (2008) observed bidirectional flows at EBs as evidence of magnetic reconnection. Recently, Chae, Moon, and Park (2003) proposed that magnetic reconnection occurs at different levels of the photosphere and the chromosphere without any preferred height.

A recent numerical simulation also supports the resistive flux emergence models described above (Isobe et al. 2007).

It presently seems, necessary to confirm the validity of the chromospheric reconnection model of EBs by high spatial resolution observations. We may obtain important clues from studies of the morphological structure of EBs and the spatial relation to the photospheric magnetic field distribution. Although the elongated structures ($\geq 1''$) of EBs were already studied by many researchers (Kurokawa et al. 1982; Georgoulis et al. 2002; Pariat et al. 2007), sub-arcsec structures have not been well known thus far. The purpose of the present work was to study the sub-arcsec structures of EBs resolved by high-resolution observations using the Hinode/Solar Optical Telescope (SOT) (Kosugi et al. 2007; Tsuneta et al. 2007; Suematsu et al. 2007; Ichimoto et al. 2004; Shimizu et al. 2007). This permitted us to follow the morphological evolution of EBs with a spatial resolution of $0.''2$, with simultaneous high-resolution data of the magnetic field.

2. Observation

Many Ca II H bright points (BPs) were observed in the active region NOAA 10933 with Hinode/SOT on 2007 January 5. Simultaneously, we succeeded to obtain good Hα filtergrams with the Domeless Solar Telescope (DST) at Hida Observatory.

Downloaded from https://academic.oup.com/pasj/article/60/3/577/1508553 by guest on 21 August 2022

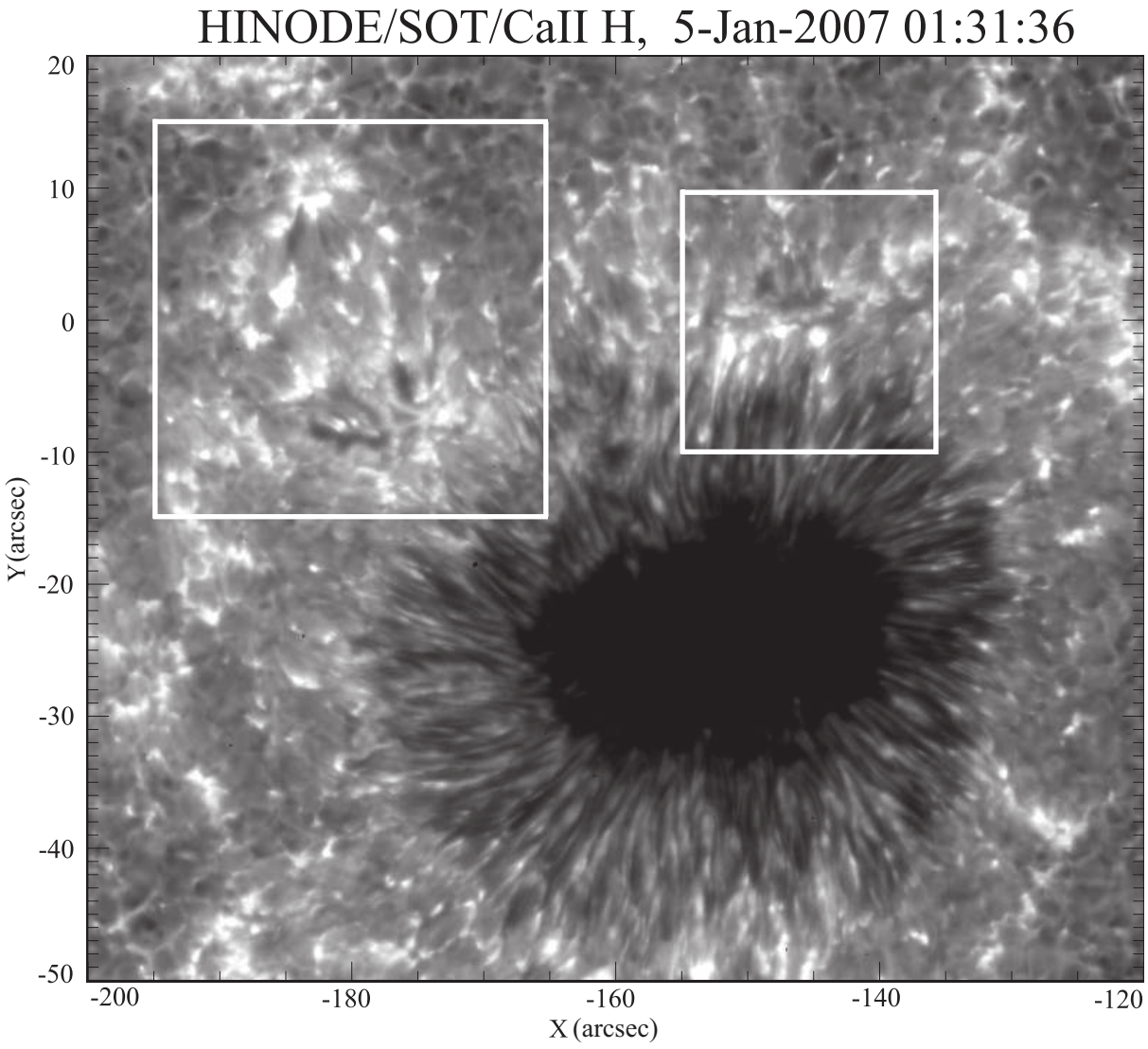

Fig. 1. Snap shot of the active region NOAA 10933 observed in Ca II H broad-band filter of Hinode/SOT. White squared regions represent an emerging flux region (left) and the north edge of the penumbra (right). In each region, we detected an EB.

Figure 1 shows a partial view ($80'' \times 70''$) of a Ca II H filtergram obtained by Hinode/SOT. This active region was located at S05 W10, and consisted of a newly emerging flux region. We can see many Ca II BPs in an emerging flux region northeast of the main spot (large square region). Some bright points can be seen at the north edge of the penumbra (small square region).

Ca II H (3968.5 Å) broad band filtergrams (passband ~ 2.2 Å) and Stokes I/V filtergrams have been analyzed. The Stokes I/V filtergrams were reduced from Fe 6302 Å filtergrams. Dark subtraction and flat-fieldings were applied in a standard manner. The cadence of filtergrams acquisition was 7 min and the spatial resolution of filtergrams was $\sim 0''.11$. At Hida Observatory, we obtained Hα center, ± 0.5 Å, ± 0.8 Å filtergrams using a Lyot filter. The cadence of Hα filtergram acquisition was nearly 2 min for each wavelength and the spatial resolution of the filtergrams was $1''$.

3. Results

We identified some of Ca II H BPs observed by Hinode/SOT with EBs. Two Ca II H BPs are considered to be EBs, because they represent the characteristic Hα spectra of EBs. The analysis in this study is concentrated on the two Ca II H BPs identified with EBs. One Ca II H BP was located in a newly developed emerging flux region (large square region in figures 1 and 2). The other was located at the edge of the penumbra (small square region in figures 1 and 2).

3.1. An Ellerman Bomb in an Emerging Flux Region

We analyzed an EB in an emerging flux region located at the northeast part of the sunspot in NOAA 10933. The flux emergence started from 18:30 UT on 2007 January 4 and lasted more than 10 hr, and finally formed two new pores. In figure 3, we show the time evolution of the Ca II H BP observed

Downloaded from https://academic.oup.com/pasj/article/60/3/577/1508553 by guest on 21 August 2022

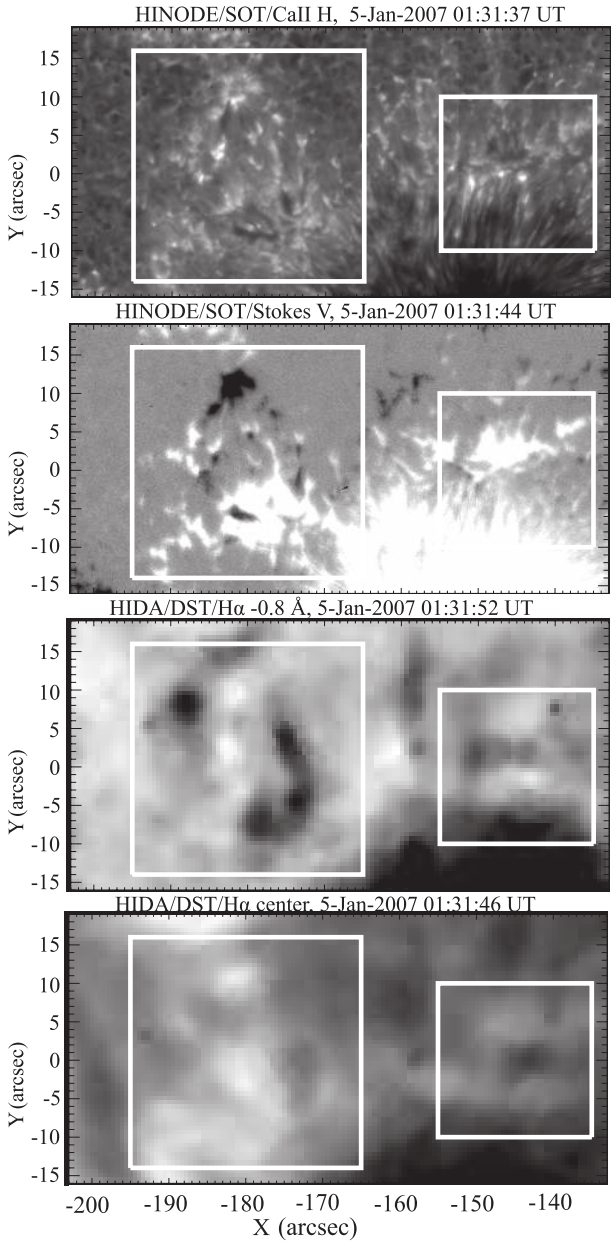

Fig. 2. Overview of the analyzed region. Each panel shows a Ca II H broad-band filter image (HINODE/SOT), the Stokes V image (HINODE/SOT), the Hα -0.8 Å image (HIDA/DST), and the Hα center image (HIDA/DST) (top to bottom). The two white squares are the same as in figure 1.

at various wavelengths. The white or black arrows in every panel show the location of the Ca II BP. From left to right, we arranged the Hα -0.8 Å, Hα center, Hα $+0.8$ Å, Ca II H, and Stokes V images. The time runs from top to bottom. In the Ca II H image of the top row, we can see a dark filament that connects Ca II H BP and the north unipolar region.

Figure 4 shows the temporal variation of the Hα intensity at the Ca II H BP. The blue, black, and red lines show Hα -0.8 Å, Hα center, and Hα $+0.8$ Å intensity profiles, respectively. The smooth lines show the low-frequency component of the noisy lines of the raw data. We plotted the intensity at the bright point subtracted by the neighboring mean intensity. The intensity enhancements in the red and blue wings are higher than that in the Hα center, so we identified the Ca II H BP with an EB. Figure 5 shows the time evolution of the emerging flux region. The images without contour lines are the Ca II H images and the images with contour lines are the Ca II H images with Stokes V contour lines. The red and blue contour lines show negative and positive polarities, respectively. The EB is located at the magnetic neutral line, as mentioned in previous studies (Fang et al. 2006; Georgoulis et al. 2002; Pariat et al. 2004, 2007).

During the evolution phase of the emerging flux region, many small bipolar structures were observed inside the emerging flux region (figure 3). The locations of these bipolar structures seem to correspond to the locations of the Ca II BPs. The temporal evolution of the EB is shown in figure 6. It has a brighter elongated core ($0\farcs65 \times 0\farcs54$) located along the magnetic neutral line of the dipole structure and a diffuse elongated halo ($1\farcs22 \times 1\farcs76$) located across the magnetic neutral line. In order to measure the size of the Ca II H feature of the EB, we used the Ca II H intensity threshold, defined by the neighboring mean intensity, $I_{\rm b}$. The halo structure is defined to have more than $1.5 \times I_{\rm b}$, while the core structure is defined to have more than $2.0 \times I_{\rm b}$. We confirmed that the halo structures had as much intensity as the Ca II H plage region, where the unipolar magnetic fields were concentrated. The spatial intensity profiles of the Ca II H BP are shown in figure 7. The left panels show the Ca II H image. The right panels show the intensity profiles along the white lines shown in the left panels. Since the observed active region was located near to the disk center, the measured sizes are expected not to be influenced by any projection effect.

In figure 8, we show the temporal development of the Ca II H intensity, the distance between the inverse polarities of the dipole, and the Stokes V flux of the Ca II H BP. The solid line with squares in the top panel is the Ca II H intensity enhancement profile normalized by the neighboring background intensity (mean active Sun). We over-plotted the Hα intensity appearing in figure 4 as a reference. We could not find any significant relation between the Hα intensity and the Ca II H intensity. The middle panel shows the variation in the distance between the inverse polarities of the dipole. The gap in the values between 01:45 and 01:52 is probably due to a newly developed negative magnetic field element approaching the EB. Compared with the Hα intensity profiles, it may be said that the EB became brighter when the distance between the inverse polarities of the dipole became shorter. The bottom panel shows the Stokes V flux variation. The solid line shows the positive one and the dotted line shows the negative one. The gap of the negative flux value between 01:45 and 01:52 is also due to a newly developed negative magnetic field element approaching the EB. During the observation, the positive polarity of the dipole did not change its flux very much, while the negative polarity of the dipole emerged and approached the positive one to dissipate and supply the magnetic energy.

3.2. *Ellerman Bombs at the Edge of the Penumbra*

We also analyzed an EB at the north edge of the penumbra. In this region, many surges were observed in the Hα filtergrams. Snap-shot images are shown in figure 9. Figure 9 also

Downloaded from https://academic.oup.com/pasj/article/60/3/577/1508553 by guest on 21 August 2022

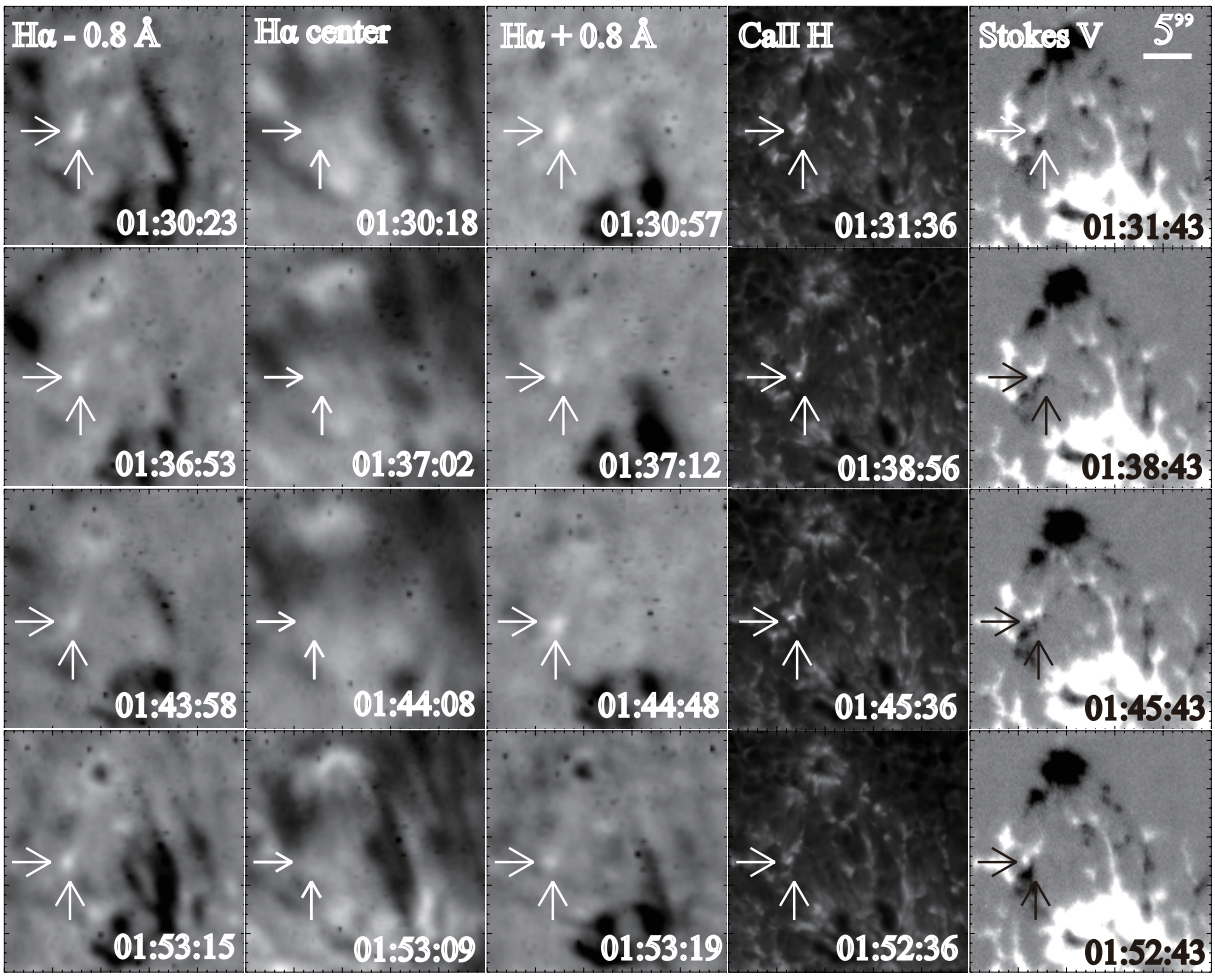

Fig. 3. Time evolution of the EB that we identified in five different wavelengths. Each row represents the Hα −0.8 Å, Hα center, Hα +0.8 Å, Ca II H broad-band filter, and Stokes V image (from left to right). Time runs from top to bottom. White and black arrows show the location of the EB.

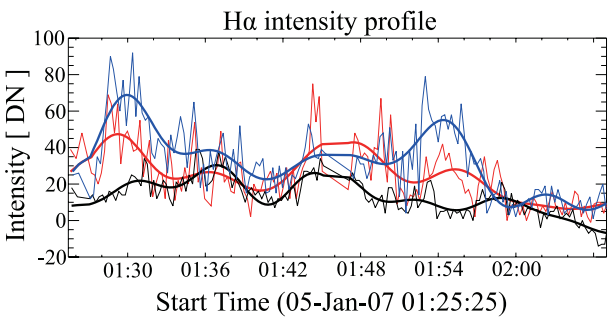

Fig. 4. Temporal variation of the Hα intensity. Blue, black, and red lines represent the intensity of Hα −0.8 Å, the Hα center, and Hα +0.8 Å, respectively.

shows a Ca II H BP located at the field-inversion line produced by a small negative polarity emerging at the positive dominant unipolar region. In figure 10, we show the Hα intensity profile of the BP in the same way as shown in figure 4. From the Hα profile, we again identified the Ca II H BP with an EB.

A magnified image of the EB (indicated by the arrow in figure 9) is shown in figure 11. The left panel shows the Ca II H image with the Stokes V contours, while the right panel shows the Stokes V image. It also has an elongated core ($0\farcs77 \times 0\farcs44$) along the field inversion line and a diffuse elongated halo ($1\farcs22 \times 1\farcs76$) across the field inversion line. We note that this small magnetic feature associated with the EB has a sub-arcsec scale, and that this small feature will disappear in a low spatial resolution observation.

4. Discussion and Conclusion

The observed EBs have two characteristic structures: bright elongated cores and diffuse halos around the cores. Both structures are located on the photospheric magnetic inversion lines. The differences between the cores and the halos are the size, the intensity, and the orientation of the major axes of their elliptic shapes. As can be seen in figure 6, contour lines of the Stokes V values nearly perfectly delineate the halo components. The size of the halo structures is $1\farcs2 \times 1\farcs8$, the intensity is more than $1.5 \times I_{\rm b}$, and the major axis is directed perpendicular to the magnetic inversion line. The halo size is nearly the same as that of the reported one by Georgoulis et al. (2002) and Pariat

Downloaded from https://academic.oup.com/pasj/article/60/3/577/1508553 by guest on 21 August 2022

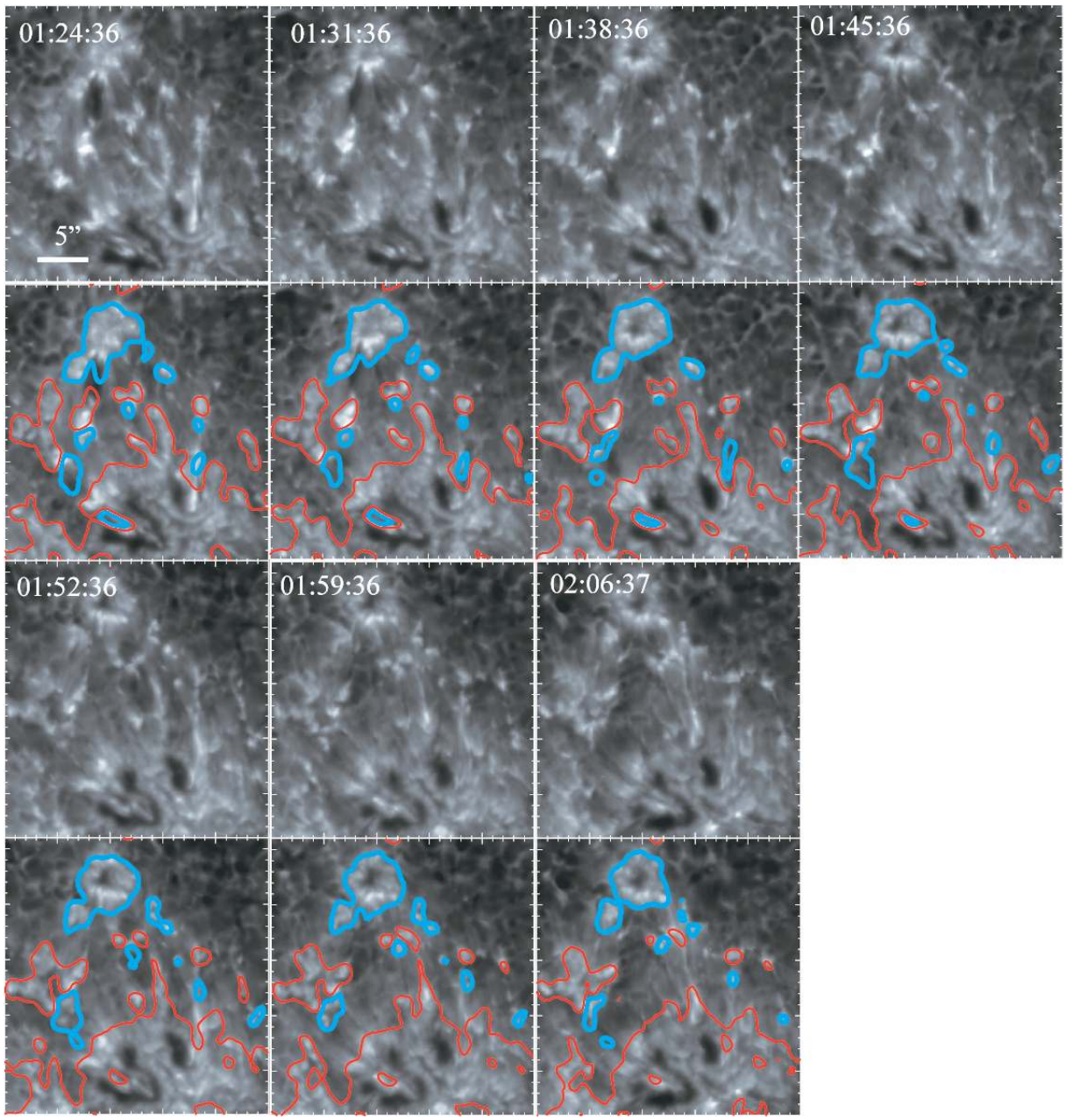

Fig. 5. Time series of Ca II H filtergrams. Images in even rows are Ca II H filtergrams with Stokes V contours. Red and blue contours show positive and negative magnetic polarities, respectively. Time is running from left to right.

Downloaded from https://academic.oup.com/pasj/article/60/3/577/1508553 by guest on 21 August 2022

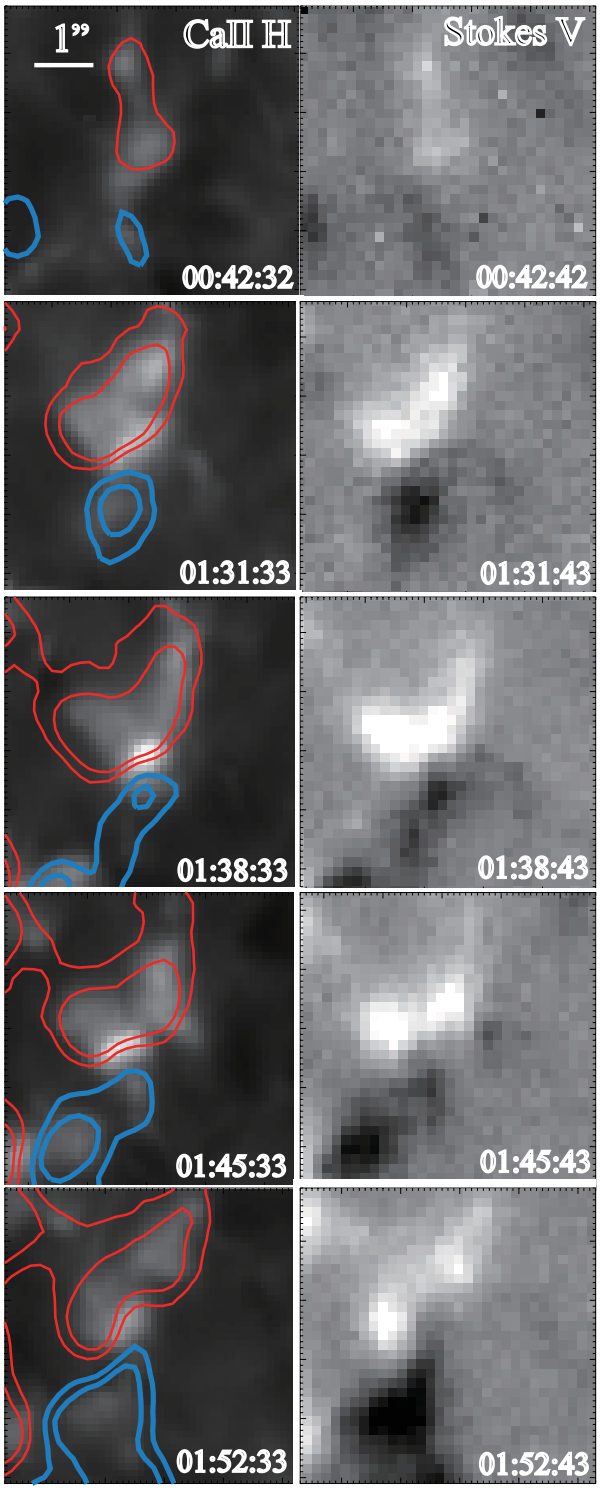

Fig. 6. Temporal variation of the Ca II H BP in the emerging flux region. Blue and red contours represent negative and positive polarities, respectively. The Ca II H BP consists of a bright elongated core ($\sim 0.''7 \times 0.''5$) and a diffuse halo. The bright core is located on the magnetic neutral line.

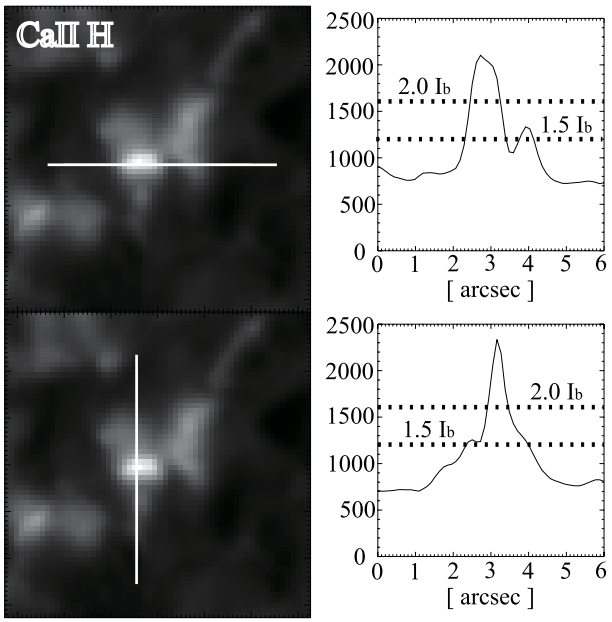

Fig. 7. Procedure to measure the size of EBs. The left panels show the Ca II H broad-band filter image around the EB. The right panels show the Ca II H intensity profiles along the white lines in the left panels. The dotted lines are $I = 1.5 \times I_b$ (lower limit of halo structure), and $I = 2.0 \times I_b$ (lower limit of core structure).

et al. (2007). On the other hand, the size of the core structures is $0.''7 \times 0.''5$, the intensity is more than $2.0 \times I_b$, and the major axis is directed parallel to the magnetic inversion line. The sub-arcsec structures of the EBs are the first to be well-observed in our observation.

Let us discuss the mechanism that produces the Ca II H core–halo structures in EBs. As observed since the 1950's, almost all of the Ca II emission was associated with magnetic fields (Leighton 1959). The halo structures observed by us are cospatial with the magnetic dipoles and their Ca II H intensities being as strong as in the unipolar quiet region. Moreover, the Ca II H intensity in the halo structures showed no significant temporal variation with EB occurrence (figure 6). We thus think that the halo structures are steadily heated, and are not directly related to the transient energy release associated with the EB itself. The heat source of the halo structures would be shock produced by downward flow along the flux tube (Shibata et al. 1989), or by any other mechanisms, such as waves.

On the other hand, the intensity of the core structures is up to nearly two-times brighter than that of the halo structures during the EBs occurrence. Thus, a further explanation might be needed. One of the possible models that could explain the core structures is shock heating produced by outflow from the magnetic reconnection point. Recently, many researchers consider that a plausible energy release mechanism of EBs is magnetic reconnection in the chromosphere or the photosphere (Kitai 1983; Ding et al. 1998; Pariat et al. 2004). Chromospheric magnetic reconnection associated with the global sea-serpentine magnetic flux tube structures was already suggested by Bernasconi et al. (2002) and Pariat et al. (2004). Takeuchi and Shibata (2001) investigated the magnetic reconnection in a highly stratified atmosphere, like the photosphere, by numerical simulation. Their simulation produced a temperature enhancement region where the reconnection outflow and the U-shaped magnetic fields above the

Downloaded from https://academic.oup.com/pasj/article/60/3/577/1508553 by guest on 21 August 2022

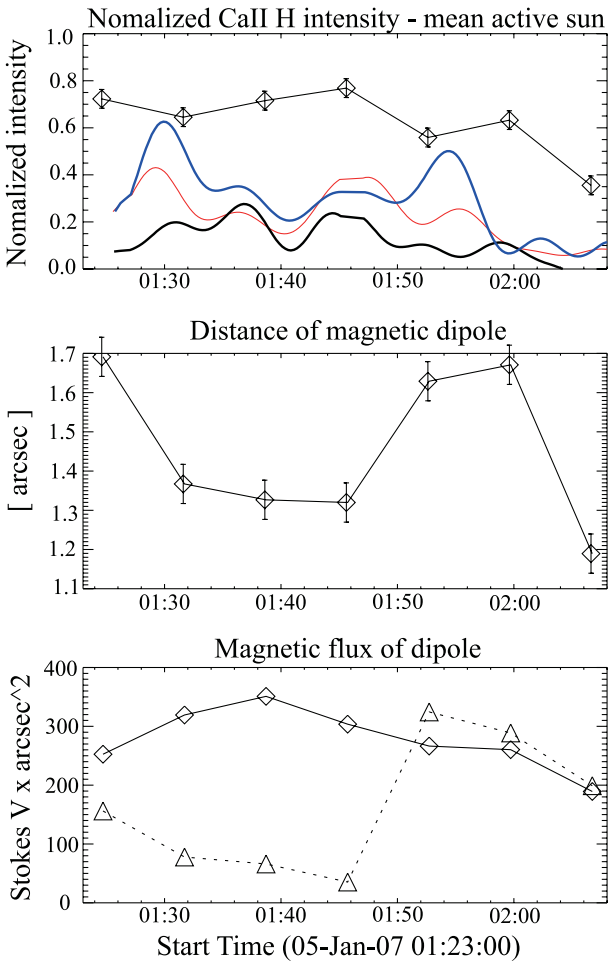

Fig. 8. Temporal development of the intensity, the distance of the dipole, and the Stokes V flux of the Ca II H bright point. The solid line with squares in the top panel is the intensity profile normalized by the background intensity. Red, black, and blue lines below show the Hα intensity profile on the same scale as in figure 4. The middle panel shows the variation in the distance between the inverse polarities of the dipole. The bottom panel shows the Stokes V flux variation. The solid line shows the positive one and the dotted line shows the negative one.

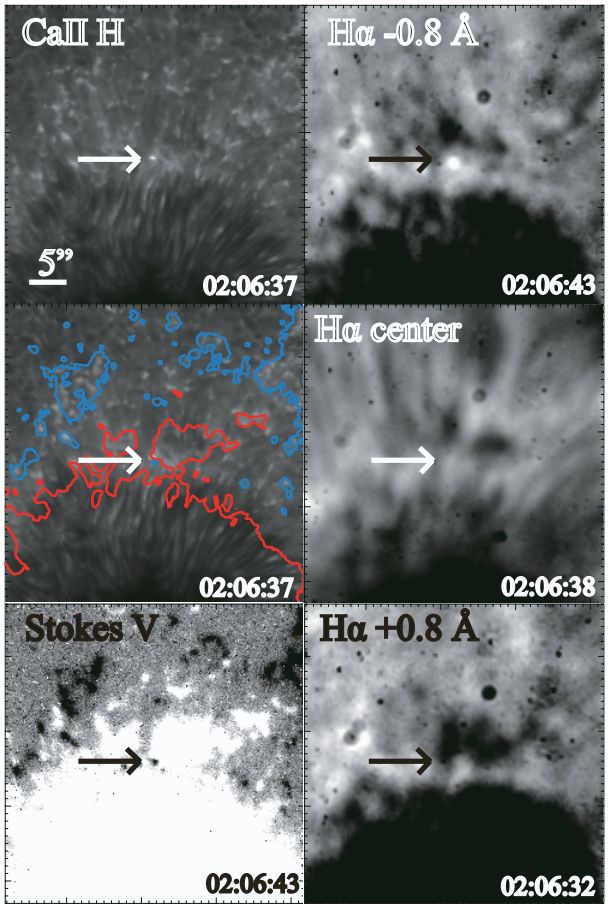

Fig. 9. EB at the north edge of the penumbra in five kinds of wavelength. The white or black arrow shows the location of the EB. The EB occurred on the magnetic neutral line produced by a small negative polarity emerging at the positive dominated magnetic field area.

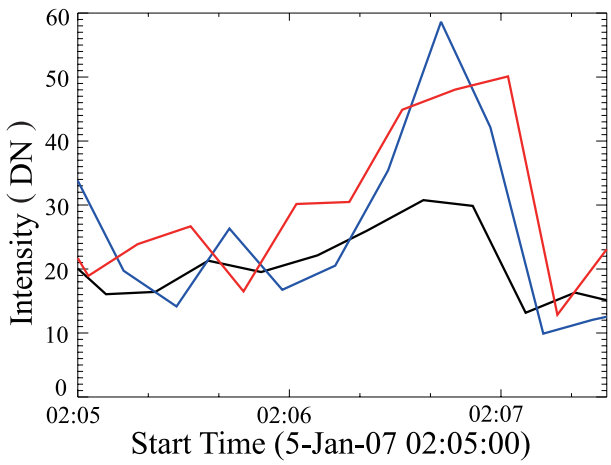

Fig. 10. Temporal variation of the Hα intensity. Blue, black, and red lines represent the intensity of Hα −0.8 Å, the Hα center, and Hα +0.8 Å, respectively.

reconnection site collided with each other. They predicted that the width of temperature enhancement is around 0.″5, which is nearly the same as what was derived from our observation. The length of the core seems to be the same as that of the magnetic neutral line (figure 6). Isobe, Tripathi, and Archontis (2007) also showed that in the process of resistive flux emergence, energy release by magnetic reconnection can indeed occur, leading to a temperature enhancement of about 1000 K above the magnetic dips. Moreover, Matsumoto et al. (2008) observed asymmetric bidirectional flow that was a characteristic feature of reconnection in the stratified atmosphere.

Therefore, it is natural to consider the core structures to be a region where the reconnection flows collide with the ambient magnetic fields, heating the atmosphere, which produce EBs (figure 12). Further observations, including vector magnetograms, are needed to verify this model.

In conclusion, we have identified some Ca II H bright points with EBs, and have discovered sub-arcsec core–halo structures in them. High-resolution observations by HINODE/SOT coordinated with simultaneous multi-wavelength observations by Hida/DST have for the first time detected this small structure

Downloaded from https://academic.oup.com/pasj/article/60/3/577/1508553 by guest on 21 August 2022

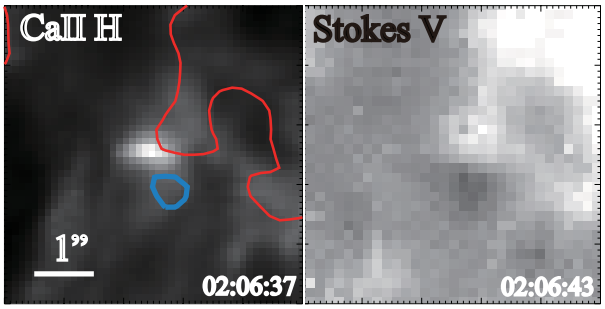

Fig. 11. Structure of the EB at the the north edge of the penumbra. The left panel is a Ca II H image. Blue and Red contours represent negative and positive polarities, respectively. The right panel is a Stokes V image.

in EBs. In order to explain this structure, we have applied the magnetic reconnection model (Pariat et al. 2004), and considered how the core–halo structures can be interpreted by this model.

The authors are grateful to all staff members of the Kwasan and Hida Observatories, Kyoto University for their guidance in our spectroscopic observations with the Domeless Solar Telescope and for the fruitful discussions with them. They are supported by a Grant-in-Aid for the 21st Century COE "Center for Diversity and Universality in Physics" from the Ministry of Education, Culture, Sports, Science and Technology (MEXT) of Japan. The authors are partially supported by the Grant-in-Aid for Creative Scientific Research The Basic Study of Space Weather Prediction (17GS0208, Head Investigator: K.Shibata) from MEXT of Japan.

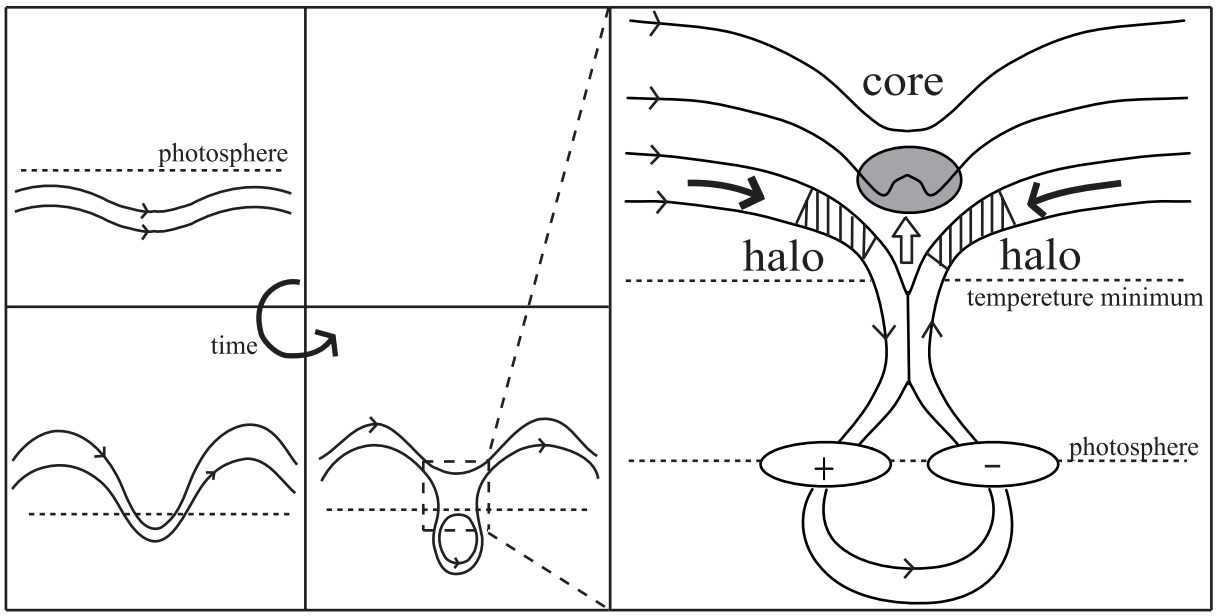

Fig. 12. One of the possible models that explain the observed core–halo structures. The core structures represent the shock region (gray-colored area) produced by reconnection flow (white arrow). The halo structures represent the shock region (shaded area) produced by downward flow (black arrows) of the loop material.

References

Bernasconi, P. N., Rust, D. M., Georgoulis, M. K., & Labonte, B. J. 2002, Sol. Phys., 209, 119
Chae, J., Moon, Y.-J., & Park, S.-Y. 2003, J. Korean Astron. Soc., 36, S13
Ding, M. D., Hénoux, J.-C., & Fang, C. 1998, A&A, 332, 761
Ellerman, F. 1917, ApJ, 46, 298
Fang, C., Tang, Y. H., Xu, Z., Ding, M. D., & Chen, P. F. 2006 , ApJ, 643, 1325
Georgoulis, M. K., Rust, D. M., Bernasconi, P. N., & Schmieder, B. 2002, ApJ, 575, 506
Hénoux, J.-C., Fang, C., & Ding, M. D. 1998, A&A, 337, 294
Ichimoto, K., et al. 2004, SPIE, 5487, 1142
Isobe, H., Tripathi, D., & Archontis, V. 2007, ApJ, 657, L53
Kitai, R. 1983, Sol. Phys., 87, 135
Kitai, R., & Muller, R. 1984, Sol. Phys., 90, 303
Kosugi, T., et al. 2007, Sol. Phys., 243, 3
Kurokawa, H., Kawaguchi, I., Funakoshi, Y., & Nakai, Y. 1982, Sol. Phys., 79, 77
Leighton, R. B. 1959, ApJ, 130, 366
Matsumoto, T., Kitai, R., Shibata, K., Otsuji, K., Naruse, T., Shiota, D., & Takasaki, H. 2008, PASJ, 60, 95
Nindos, A., & Zirin, H. 1998, Sol. Phys., 182, 381
Pariat, E., Aulanier, G., Schmieder, B., Georgoulis, M. K., Rust, D. M., & Bernasconi, P. N. 2004, ApJ, 614, 1099
Pariat, E., Schmieder, B., Berlicki, A., Deng, Y., Mein, N., López Ariste, A., & Wang, S. 2007, A&A, 473, 279
Roy, J.-R. 1973, Sol. Phys., 28, 95
Shibata, K., Tajima, T., Matsumoto, R., Horiuchi, T., Hanawa, T., Rosner, R., & Uchida, Y. 1989, ApJ, 338, 471
Shimizu, T., et al. 2008, Sol. Phys., 249, 221
Suematsu, Y., et al. 2008, Sol. Phys., 249, 197
Takeuchi, A., & Shibata, K. 2001, ApJ, 546, L73
Tsuneta, S., et al. 2008, Sol. Phys., 249, 167
Zachariadis, TH. G., Alissandrakis, C. E., & Banos, G. 1987, Sol. Phys., 108, 227

Downloaded from https://academic.oup.com/pasj/article/60/3/577/1508553 by guest on 21 August 2022